Tan, D.-B., et al., 2022, Differentiation between carbonate and silicate metasomatism based on lithium isotopic compositions of alkali basalts: Geology, v. 50, https://doi.org/10.1130/G50090.1

Supplementary Information Appendix for

Differentiation between carbonate and silicate metasomatism based on lithium isotopic compositions of alkali basalts

Dong-Bo Tan[1], Yilin Xiao[1, 2*], Li-Qun Dai[1, 2*], He Sun[3], Yangyang Wang[1], Hai-Ou Gu[3]

[1] *CAS Key Laboratory of Crust-Mantle Materials and Environments, School of Earth and Space Sciences, University of Science and Technology of China, Hefei 230026, China.*

[2]*CAS Center of Excellence in Comparative Planetology, China.*

[3]*Hefei University of Technology, School of Resources and Environmental Engineering, Hefei, 230009, China*

*Corresponding author: *Yilin Xiao (ylxiao@ustc.edu.cn);*

Li-Qun Dai (lqdai@ustc.edu.cn)

This file contains:

- Analytical methods
- Table DR1-4
- Figures DR1-6
- References

ANALYTICAL METHODS

Li concentration and Li isotopic values were analyzed for a suite of 44 West Qinling samples including 18 MABs and 26 CABs. Li isotopic analyses were completed at the CAS Key Laboratory of Crust-Mantle Materials and Environments, University of Science and Technology of China, and School of Resources and Environmental Engineering, Hefei University of Technology. The procedures of dissolving, column, and isotopic analysis have been detailed reported on Sun et al. (2018). Briefly, ~50 mg whole-rock sample powders were dissolved in screw-top beakers by mixing of optima-grade concentrated HF-HNO_3-HCl. After a series of steps of dissolving and drying, clear solutions were obtained and used for column geochemical separation. Separation efficiency was checked by ICP-MS, aiming to guarantee the Na/Li ratios <3 and recovery >99.9%. Finally, Li isotopic compositions were determined by the standard-sample bracketing method using a Nu Plasma multi-collector inductively coupled plasma mass spectrometry (MC-ICP-MS). The reference materials BHVO-2G and BCR-2G were processed through whole processes with samples for accuracy check, and yield δ^7Li values of +4.4 ± 0.3‰ for BHVO-2G and -0.8 ± 0.3‰ for BCR-2G, consistent with reported values (Magna et al., 2006).

TABLE DR1-4

Table. 1. The Li isotopic compositions of Cenozoic alkali basalts and Mesozoic alkali basalts from West Qingling orogen

Locations	Sample NO.	Li ((μg/g)	δ^7Li (‰)
Haoti	14HT01	12.3	7.1
	14HT02	13.9	5.7
	14HT03	14.3	6.0
	14HT04	8.88	4.2
	14HT05	9.47	5.9
	14HT07	11.3	4.1
	14HT08	20.4	7.5
	14HT10	10.9	5.6
Caihua	14LX01	19.1	7.6
	14LX03	14.3	8.8
	14LX04	22.5	5.2
	14LX05	10.0	4.3
Fenshui	14FS01	21.0	11.2
	14FS02	13.0	8.1
	14FS03	18.8	4.4
	14FS04	12.8	9.2
	14FS05	20.5	6.1
	14FS06	16.6	8.4
	14LX06	13.9	8.2
	14LX11	27.7	3.2
	14LX17	12.5	9.6
	14LX18.	12.2	8.9
	14LX22	10.3	7.4
	14LX23	9.54	7.4
	14LX24	9.15	7.7
	14LX25	16.5	5.6

Locations	Sample NO.	Li ((μg/g)	δ^7Li (‰)
Madang	12LZ02	22.6	-3.3
	12LZ04	23.4	-2.4
	12LZ05	24.5	-2.9
	12LZ06	19.4	-1.9
Ganjia	12LZ08	27.0	2.2
	12LZ12	30.0	1.4
	12LZ13	43.3	3.4
	12LZ14	18.6	4.7
	12LZ17	24.5	-0.5
	12LZ18	26.5	-0.1
	12LZ19	32.7	-0.7
Duomaohe	12LZ24	101	0.1
	12LZ25	69.7	2.0
	12LZ26	92.0	2.4
	12LZ28	82.2	1.0
	12LZ23	66.0	-1.7
	12LZ29	64.3	-0.2
	12LZ30	67.4	-1.0
Standards	BHVO-2G	3.69	4.3
	GSP-2	42.5	-0.9

Table. 2. The major and trace elements of Cenozoic alkali basalts and Mesozoic alkali basalts from West Qingling orogen

Locations	Haoti								Caihua				Fenshui													
Sample NO.	14H T01	14H T02	14H T03	14H T04	14H T05	14H T07	14H T08	14H T10	14L X01	14L X03	14L X04	14L X05	14F S01	14F S02	14F S03	14F S04	14F S05	14F S06	14L X06	14L X11	14L X17	14L X18.	14L X22	14L X23	14L X24	14L X25
Major elements (wt. %)																										
SiO_2	39.7	38.6	39	39	39.1	39.5	40.1	39	39.9	39.8	39.5	39.2	38	38	38.6	38.1	38.9	37.4	36.9	40.8	39	39.1	39.7	39	38.6	38.9
Al_2O_3	9.34	9.08	9.13	9.16	9.2	9.3	9.51	9.11	9.31	9.73	9.5	9.52	7.41	7.49	7.43	7.49	7.5	7.3	7.44	8.01	7.89	7.89	8.25	7.89	7.78	7.68
Fe_2O_3	12.1	12.3	12.5	12.4	12.4	12.3	12.1	12.4	11.9	11.5	11.7	11.4	10.8	10.8	10.7	10.8	11.1	10.8	10.8	11.4	11.4	11.5	11.2	11.1	10.9	11
CaO	13.2	13.3	13	13	12.9	13	12.4	13.2	13.5	14.6	14.1	14.7	14.8	14.8	14.8	14.5	14.2	15.1	16.3	13.5	12.7	12.5	13.6	14	14.1	14
MgO	12.7	13	13	13	12.9	13	12.4	13.2	13.2	11.9	12.6	12.1	16.4	15.8	16.1	16.5	16.5	16.3	14.7	14.1	17.7	17.9	15.3	16	16	16.3
Na_2O	2.91	2.66	2.77	3.63	2.58	3.4	2.55	3.06	2.61	2.65	2.24	2.42	0.72	1.66	2	1.75	1.82	1.54	1.68	0.96	1.54	1.63	1.37	1.98	1.62	0.6
K_2O	2.18	2.77	2.71	3.06	3.68	2.62	2.42	3.01	1.84	1.8	2.07	1.72	0.4	1	1.19	1.12	0.99	1.02	1.05	0.74	1.24	1.51	0.92	1.21	1.18	0.26
Cr_2O_3	0.04	0.04	0.05	0.05	0.04	0.05	0.04	0.05	0.04	0.03	0.05	0.03	0.09	0.09	0.09	0.09	0.09	0.09	0.09	0.09	0.08	0.09	0.08	0.08	0.09	0.09
TiO2	3.75	3.87	3.94	3.91	3.89	3.81	3.84	3.89	3.52	3.29	3.33	3.28	3.01	3.01	3.02	3.01	3.11	3	3.03	3.21	2.94	2.92	3.23	3.17	3.12	3.08
MnO	0.17	0.18	0.18	0.18	0.18	0.18	0.17	0.18	0.16	0.16	0.16	0.16	0.15	0.15	0.15	0.15	0.15	0.15	0.15	0.16	0.17	0.17	0.16	0.16	0.15	0.16
P_2O_5	0.97	1.36	1.3	1.22	1.31	1.21	0.98	1.4	1.02	1.2	1.06	1.24	1.19	1.24	1.01	1.1	1.28	1.32	1.52	1.62	1.36	1.44	1.22	1.27	1.3	1.4
LOI	2.02	1.69	1.68	0.94	1.14	1.12	2.23	0.9	2.42	2.97	3.3	3.12	6.43	5.14	4.17	4.58	3.95	5.55	6.42	5.03	3.36	3.26	5.45	4.26	4.95	6.29
Total	99.08	98.85	99.26	99.55	99.32	99.49	98.74	99.4	99.4	99.7	99.61	98.89	99.3	99.18	99.26	99.2	99.6	99.5	100	99.6	99.38	99.91	100.4	100.0	99.79	99.76
Trace elements ((μg/g)																										
Ba	978	1385	1538	1456	1343	1158	1220	126	910	1480	915	1823	809	730	787	1279	781	714	1195	1039	1329	1428	1086	1128	1183	1692
Rb	43.4	85.3	79.2	83.5	89.3	71.3	62.1	74.8	42.2	49	81.1	53.9	12.2	28.3	31.7	27.9	26.5	26.5	26.8	37.4	43.7	50.4	28.9	34.7	35.5	20.8
Sr	1409	1841	1806	1724	1685	1669	1700	1691	1260	1288	1304	1455	1992	1514	1692	1787	1742	1864	1410	1129	1409	1483	1475	1399	1453	2035
Ta	6.64	7.4	7.23	7.29	7.12	7.01	6.67	7.15	6.13	6.02	5.65	6.1	5.62	5.77	5.88	5.86	5.88	5.72	5.9	5.98	6.15	6.15	5.9	5.66	5.71	5.75
Nb	133	148	147	149	143	139	128	143	126	131	122	129	128	131	126	129	129	127	133	134	130	127	132	127	127	124
Hf	8.07	9	9.06	8.97	8.93	8.33	8.68	8.54	7.11	6.65	5.99	6.41	7.48	7.66	7.48	7.65	7.59	7.64	7.95	8.09	6.83	6.58	8.07	7.93	7.68	7.58
Zr	389	428	447	436	429	399	405	405	332	316	291	301	361	364	343	364	359	353	379	394	334	317	389	376	371	360

Y	34	37.8	36.6	37.5	37.6	36.2	34.6	36.2	30.7	30.3	28.1	30	29	32	30.4	30.6	30.8	31.6	31.7	32	29.9	29.2	32.7	31	31	30.7
Th	11.9	12.8	12.4	12.6	12.6	12.4	11.5	12.3	12	13.1	12	13.6	13.8	14	14.6	14.6	14.7	14.5	14.7	15.1	14.2	14.4	14.9	14.6	14.8	15.2
U	2.61	2.94	3.01	2.89	2.88	2.78	2.55	2.92	2.55	2.89	2.59	2.75	3.08	3.15	3.11	3.14	3.11	3.13	3.39	3.57	3.13	3.16	3.12	3.07	3.17	3.05
Cr	294	305	296	304	292	305	278	301	318	229	320	239	615	610	624	739	603	653	589	615	613	604	551	543	576	640
Ni	306	305	297	316	277	321	299	316	322	256	336	245	505	498	511	511	510	529	487	472	508	516	454	437	440	501
Sc	19.7	19.3	18.9	19.2	19.1	19.4	19.5	19.2	19.1	19.1	18.2	19.6	16.4	16.3	17.5	17	16.9	17	16.9	17.6	18.6	18.6	17.6	17.2	17.2	17.1
V	200	208	211	198	202	208	196	205	199	196	196	193	150	153	150	151	147	153	161	165	186	181	160	152	151	148
Cu	67.1	50.5	68.7	60.2	49.6	61.9	58.2	49	84.2	66.4	104	61.1	72.3	75	58.9	65.8	72.1	81.6	93	72.7	81.1	76.3	71.5	66.4	65.7	74.2
Pb	4.94	5.18	5.38	1.83	5.04	4.46	5.32	4.26	5.25	6.11	5.11	5.8	4.92	5.11	4.34	4.29	4.29	4.76	5.48	4.02	6.17	6.06	5.82	5.56	4.83	5.15
Zn	119	128	124	126	122	123	120	124	115	115	110	115	107	112	107	110	112	109	110	116	116	115	118	115	115	112
Li	12	12.4	13.6	8.86	9.48	8.01	20.4	9.7	17.7	14.9	21.3	9.89	19.3	11.5	18.8	12.3	19.6	15.3	12.6	25.8	11.3	11.6	10.7	8.98	8.73	14.8
Co	54.6	55.7	55	57.2	53	55.3	54	57.2	55.2	53.5	57.4	51.4	57.6	57.4	58.4	58.5	59.9	58.4	57.1	57.3	60.5	61.1	55.8	54.2	54.9	56.3
Ga	18.3	20.5	19.7	18.8	18.3	18.3	19	19.1	17.5	18	18	18	15.1	14.8	15.2	15.3	15.1	14.8	15.1	13.3	14.8	14.9	15.7	14.8	14.6	12.8
La	94.1	104	99.7	102	101	99.2	92.5	102	93.4	98.8	91	103	111	113	115	116	118	115	118	119	105	106	117	114	115	116
Ce	176	193	189	191	189	183	174	191	171	180	164	184	206	208	217	216	218	215	220	227	197	197	224	217	220	223
Pr	20.3	22.5	21.9	21.9	21.8	21.5	20	21.8	19.5	20.2	18.4	20.7	23.3	24.1	24.8	24.6	25.1	24.7	25.3	26.1	22.5	22.8	25.9	25.2	25.5	25.8
Nd	80.5	90.1	87.3	88.8	86.5	86.3	80.6	87.1	75.6	77.8	70.6	78.9	90	94.5	95.4	96	96.5	96.3	97.9	97.2	83.2	84.1	97.3	95.1	97	96.5
Sm	15.5	17.3	16.6	17	16.6	16.6	15.3	16.4	14.4	14	131	143	16.2	167	171	17	17.1	17.4	17.2	17.3	147	149	178	173	174	175
Eu	4.55	5.18	4.96	5.08	4.95	4.93	4.64	4.95	4.25	4.25	3.94	4.36	4.73	4.88	5.09	5.06	5.12	5.2	5.11	5.04	4.37	4.36	5.07	4.98	5.02	5.12
Gd	12.2	13.5	12.9	13.4	12.8	13.2	12.4	13.1	11.2	11.3	10.2	11.2	11.9	12.4	12.9	12.5	12.8	13	13	13.2	11.3	11.2	13.5	13.1	12.9	13
Tb	1.58	1.77	1.72	1.74	1.74	1.69	1.64	1.72	1.46	1.41	1.34	1.44	1.5	1.54	1.58	1.55	1.59	1.64	1.62	1.66	1.49	1.49	1.66	1.6	1.6	1.63
Dy	7.79	8.7	8.39	8.59	8.44	8.3	8.12	8.21	7.24	6.88	6.55	7.09	7.05	7.42	7.47	7.37	7.33	7.49	7.62	7.72	6.83	6.9	7.82	7.53	7.61	7.61
Ho	1.24	1.36	1.34	1.31	1.33	1.31	1.3	1.35	1.15	1.12	1.06	1.16	1.07	1.18	1.16	1.16	1.18	1.18	1.21	1.21	1.13	1.09	1.21	1.17	1.16	1.16
Er	2.85	3.03	3.06	3.1	2.89	2.9	2.99	2.95	2.62	2.63	2.37	2.53	2.38	2.43	2.44	2.45	2.51	2.62	2.62	2.76	2.74	2.61	2.86	2.78	2.78	2.7
Tm	0.35	0.37	0.36	0.35	0.35	0.34	0.34	0.36	0.31	0.3	0.27	0.31	0.27	0.3	0.3	0.29	0.3	0.3	0.32	0.31	0.31	0.31	0.33	0.32	0.32	0.32
Yb	1.96	2.04	1.99	1.95	2	1.91	1.89	1.97	1.77	1.72	1.61	1.7	1.54	1.58	1.55	1.59	1.59	1.65	1.62	1.68	1.74	1.7	1.77	1.69	1.6	1.64
Lu	0.25	0.26	0.27	0.26	0.25	0.24	0.26	0.26	0.23	0.22	0.21	0.22	0.2	0.22	0.2	0.21	0.21	0.19	0.2	0.22	0.23	0.22	0.24	0.22	0.22	0.22
Y	34	37.8	36.6	37.5	37.6	36.2	34.6	36.2	30.7	30.3	28.1	30	29	32	30.4	30.6	30.8	31.6	31.7	32	29.9	29.2	32.7	31	31	30.7

Locations	Madang				Ganjia							Duomaohe						
Sample NO.	12LZ02	12LZ04	12LZ05	12LZ06	12LZ08	12LZ12	12LZ13	12LZ14	12LZ17	12LZ18	12LZ19	12LZ24	12LZ25	12LZ26	12LZ28	12LZ23	12LZ29	12LZ30
Major elements (wt. %)																		
SiO_2	41.74	42.04	42.7	41.41	45.66	44.11	44.46	44.72	44.26	44.17	44.16	42.07	42.66	42.99	43.23	42.68	42.34	42.39
Al_2O_3	14.4	14.97	15.12	14.66	15.82	14.3	15.71	15.55	14.19	14.28	14.17	12.39	12.45	12.58	12.64	12.45	12.31	12.34
Fe_2O_3	10.79	11.07	10.73	10.1	10.44	10.84	9.98	10.46	10.86	10.7	10.69	12.24	12.1	12.16	11.89	12.08	12.21	12.32
CaO	10.65	9.88	9.31	10.42	8.79	9.05	8.86	9.17	8.87	8.7	8.74	10.04	9.96	10.66	10.27	9.87	9.95	10.09
MgO	9.03	8	7.18	8.62	7.2	10.28	7.89	8.86	11.09	10.59	10.71	10.48	10.56	9.25	9.66	10.95	10.94	10.77
Na_2O	2.51	2.78	3.11	2.59	2.69	2.74	3.37	3.28	2.52	2.47	2.53	3.2	3.61	3.3	3.45	3.51	3.32	3.51
K_2O	0.43	0.59	0.58	0.57	1.5	0.78	1.11	1.47	1	0.82	0.88	0.68	0.53	0.64	0.63	0.7	0.72	0.7
Cr_2O_3	0.06	0.04	0.03	0.06	0.04	0.06	0.05	0.04	0.07	0.06	0.06	0.05	0.05	0.06	0.06	0.05	0.05	0.05
TiO2	2.41	2.67	2.6	2.51	2.21	2.36	2.5	2.47	2.25	2.29	2.27	2.84	2.8	2.75	2.68	2.86	2.82	2.84
MnO	0.13	0.14	0.11	0.14	0.23	0.16	0.15	0.15	0.16	0.16	0.15	0.16	0.16	0.15	0.16	0.16	0.17	0.17
P_2O_5	0.455	0.511	0.543	0.481	0.409	0.497	0.47	0.463	0.475	0.471	0.464	0.706	0.686	0.693	0.673	0.695	0.688	0.697
LOI	7.81	7.83	8.5	8.48	5.27	5.2	5.65	3.5	4.7	5.68	5.42	5.63	4.97	5.44	5.02	4.57	4.86	4.51
Total	100.4	100.5	100.5	100	100.3	100.4	100.2	100.1	100.4	100.4	100.2	100.5	100.5	100.7	100.4	100.6	100.4	100.4
Trace elements (μg/g)																		
Ba	130	168	174	143	178	233	592	181	219	287	402	472	442	426	418	461	473	460
Rb	1.74	4.45	5.91	3.57	17.9	3.63	9.84	11.7	6.07	5.44	5.18	3.99	3.2	3.18	3.68	3.71	4.08	3.79
Sr	848	954	993	888	624	671	930	1209	667	652	658	903	813	877	826	844	828	867
Ta	2.03	2.43	2.44	2.11	1.62	2.31	1.94	1.95	2.2	2.21	2.24	3.88	3.7	3.56	3.49	3.78	3.79	3.84
Nb	33	39.7	39.8	34.5	26.3	38.3	31.8	32.2	36.4	36.5	37.3	64.9	62	59.6	59.1	63.9	63.5	64.1
Hf	4.33	4.84	4.91	4.42	4.28	4.69	4.36	4.37	4.59	4.6	4.66	5.91	5.7	5.72	5.55	5.79	5.9	5.81
Zr	203	229	234	209	193	219	211	213	211	212	216	258	249	250	246	255	257	258
Y	23	25.2	24.5	24.2	25.5	22.9	26.1	26.2	22.4	22.9	23.7	23.5	22.9	23.9	23.6	23.6	23.8	24
Th	1.85	2.21	2.31	2.02	2.61	2.85	1.81	1.76	2.69	2.81	2.89	4.59	4.42	4.58	4.53	4.73	4.62	4.68
U	0.74	0.9	0.92	0.8	0.67	0.96	0.75	0.76	0.94	0.96	0.98	1.46	1.49	1.51	1.52	1.51	1.6	1.51
Cr	419	338	283	418	272	428	326	342	482	490	475	380	380	414	413	388	388	394

Ni	272	231	195	303	129	235	171	180	262	258	250	232	234	238	237	236	246	237
Sc	21.8	23.1	23.1	26.8	21.8	19.1	22.5	18.2	16.5	19.7	21.2	14.5	13.9	18	16	17.6	14.9	17.3
V	210	226	220	214	198	219	218	218	216	218	222	263	248	251	247	253	254	257
Cu	55.8	50.7	38.2	36.7	73.8	54.1	52.4	56.2	51.2	50.9	54.1	45.1	46.8	53	53.8	51.6	58.2	53.2
Pb	1.77	2.5	2.47	2.35	3.48	3.47	2.03	2	3.29	3.44	3.64	5.47	4.49	3.79	4.88	4.39	3.44	3.75
Zn	66.5	72.3	72.7	76.5	87.9	80.2	68.5	68.1	78.5	79.9	80.1	107	104	107	105	106	107	108
Li	22	22.6	22.8	20.1	25.2	26.2	42.9	17	25.5	26.4	29.6	99.8	69.4	94.8	73.8	60.5	65.9	58.7
Co	51.3	52	51.8	58	42.5	49.7	43.5	45.1	52.1	51.5	51	54.6	54.3	54.3	54.1	54.9	56.5	56.2
Ga	16.9	18.6	18.4	17.5	19.6	19.7	17.5	18.1	19.1	18.9	19.3	21.8	21.6	21.6	21.5	21.7	22	22.1
La	21.5	25.3	25.5	22.7	20.6	26.3	21	21	24.6	25	25.7	39.8	38.2	38.5	37.7	39	39.6	39.6
Ce	45.2	52.8	53.5	48.3	44.5	54.5	45.2	45	51.5	52.5	54	81.8	79.5	80.2	77.9	81	81.8	81.9
Pr	5.57	6.33	6.38	5.75	5.51	6.56	5.56	5.51	6.21	6.31	6.47	9.7	9.5	9.5	9.26	9.69	9.87	9.76
Nd	23	26.4	26.4	23.9	23	26.8	23.8	23.3	25.7	26.2	26.8	40.3	38.8	38.8	38.1	39.7	39.7	40.1
Sm	5.24	5.91	5.91	5.17	5.45	5.99	5.21	5.38	5.78	5.87	6.01	8.46	7.99	8.25	8.04	8.2	8.22	8.46
Eu	1.77	2.02	1.94	1.83	1.77	1.87	1.9	1.87	1.84	1.86	1.93	2.52	2.46	2.53	2.38	2.48	2.57	2.56
Gd	5.17	5.74	5.56	5.28	5.55	5.61	5.56	5.52	5.41	5.42	5.64	7.05	6.94	7.05	6.85	6.99	7.14	7.24
Tb	0.8	0.87	0.85	0.82	0.86	0.86	0.88	0.88	0.81	0.83	0.85	1.01	0.96	0.98	0.95	0.99	0.98	1.01
Dy	4.55	4.96	4.74	4.52	4.86	4.73	5.04	4.96	4.51	4.59	4.82	5.2	5.06	5.2	5.08	5.01	5.34	5.31
Ho	0.88	0.95	0.93	0.89	0.96	0.87	1	0.96	0.85	0.85	0.87	0.89	0.9	0.91	0.9	0.9	0.9	0.93
Er	2.34	2.38	2.46	2.42	2.55	2.26	2.54	2.65	2.15	2.25	2.33	2.23	2.21	2.26	2.28	2.23	2.31	2.2
Tm	0.33	0.35	0.34	0.33	0.37	0.31	0.38	0.37	0.29	0.3	0.32	0.29	0.28	0.29	0.3	0.28	0.3	0.29
Yb	1.99	2.07	2.14	2.08	2.2	1.85	2.38	2.19	1.81	1.93	1.97	1.66	1.58	1.72	1.69	1.62	1.66	1.71
Lu	0.29	0.3	0.29	0.3	0.33	0.27	0.33	0.34	0.27	0.27	0.29	0.21	0.21	0.24	0.22	0.23	0.24	0.23
Y	23	25.2	24.5	24.2	25.5	22.9	26.1	26.2	22.4	22.9	23.7	23.5	22.9	23.9	23.6	23.6	23.8	24

Note: Major and trace element concentrations are from Dai et al., (2014, 2017; 2018)

Table. 3. The Sr-Nd-Hf-Mg isotopic compositions of Cenozoic alkali basalts and Mesozoic alkali basalts from West Qingling orogen

Locations	Sample NO.	Rb (ppm)	Sr(ppm)	$^{87}Rb/^{86}Sr$	$^{87}Sr/^{86}Sr$	$(^{87}Sr/^{86}Sr)$	Sm (ppm)	Nd (ppm)	$^{147}Sm/^{144}Nd$	$^{143}Nd/^{144}Nd$	$e_{Nd}(t)$	T_{DM} (Ma)	Lu	Hf	$^{176}Lu/^{177}Hf$	$^{176}Hf/^{177}Hf$	eHf(t)	TDM1	$\delta^{26}Mg$ (‰)
Haoti	14HT01	43.4	1409	0.0891	0.704082	0704053	15.5	80.5	0.116303	0.512891	5.2	406	0.25	8.07	0.00434	0.282979	7.8	425	-0.41
	14HT03	79.2	1806	0.1268	0.704167	0704125	16.6	87.3	0.114728	0.512873	4.9	427	0.27	9.06	0.00426	0.282972	7.4	435	
	14HT05	89.3	1685	0.1533	0.703835	0703784	16.6	86.5	0.116387	0.512855	4.5	464	0.25	8.93	0.0039	0.282987	7.9	408	-0.41
	14HT08	62.1	1700	0.1057	0.703776	0703742	15.3	80.6	0.114748	0.512878	5	420	0.26	8.68	0.00431	0.282984	7.8	417	-0.46
	14HT10	74.8	1691	0.1279	0.70388	0703838	16.4	87.1	0.114026	0.512863	4.7	439	0.26	8.54	0.00435	0.282969	7.3	440	-0.54
Caihua	14LX01	42.2	1260	0.097	0.70413	0.704098	14.4	75.6	0.115	0.512841	4.2	477	0.23	7.11	0.005	0.282956	7	463	
	14LX03	45.4	1537	0.085	0.704801	0.704773	14.2	76.3	0.113	0.512797	3.4	533	0.23	6.75	0.005	0.282925	5.8	518	
	14LX04	81.1	1304	0.1799	0.704316	0704257	13.1	70.6	0.112105	0.512817	3.8	500	0.21	5.99	0.00508	0.282951	6.6	479	-0.36
Fenshui	14FS01	12.2	1992	0.018	0.705621	0.705615	16.2	90	0.109	0.512809	3.6	495	0.2	7.48	0.004	0.282959	7.1	449	
	14FS03	31.7	1692	0.0543	0.704747	0704729	17.1	95.4	0.108113	0.512818	3.8	481	0.2	7.48	0.00372	0.282967	7.2	436	-0.32
	14LX06	26.8	1410	0.055	0.70466	0.704642	17.2	97.9	0.106	0.512817	3.8	471	0.2	7.95	0.004	0.282958	7	448	
	14LX11	37.4	1129	0.096	0.704551	0.70452	17.3	97.2	0.108	0.512804	3.5	498	0.22	8.09	0.004	0.282957	7	453	
	14LX17	43.7	1409	0.0897	0.704435	0704406	14.7	83.2	0.106468	0.512805	3.6	492	0.23	6.83	0.00477	0.282923	5.6	519	
	14LX18.	50.4	1483	0.0983	0.70427	0704238	14.9	84.1	0.107086	0.512801	3.5	499	0.22	6.58	0.0048	0.282923	5.6	520	-0.35
	14LX23	34.7	1399	0.0718	0.704262	0704239	17.3	95.1	0.109693	0.512807	3.6	503	0.22	7.93	0.00396	0.282963	7	446	-0.36
	14LX25	20.8	2035	0.0296	0.704041	0704031	17.5	96.5	0.109571	0.512803	3.5	509	0.22	7.58	0.00417	0.282953	6.7	463	-0.38
Madang	12LZ02	1.74	848	0.0059	0.703513	0.703504	5.24	23	0.137863	0.51301	8	281	0.29	4.33	0.00951	0.283111	13.6	256	-0.21
	12LZ06	3.57	888	0.0116	0.703761	0.703745	5.17	23.9	0.131069	0.513013	8.2	253	0.3	4.42	0.00958	0.283108	13.5	263	-0.32
Ganjia	12LZ12	3.63	671	0.0156	0.703712	0.70369	5.99	26.8	0.135229	0.512922	6.3	443	0.27	4.69	0.00808	0.283053	11.6	347	-0.3
	12LZ13	9.84	930	0.0306	0.705368	0.705324	5.21	23.8	0.132339	0.513001	7.9	280	0.33	4.36	0.01077	0.283104	13.2	283	
	12LZ14	11.7	1209	0.0279	0.705801	0.705761	5.38	23.3	0.139662	0.513012	8	286	0.34	4.37	0.01089	0.283104	13.2	284	-0.29
	12LZ17	6.07	667	0.0263	0.70369	0.703652	5.78	25.7	0.135725	0.51292	6.3	450	0.27	4.59	0.00823	0.283048	11.4	358	
	12LZ19	5.18	658	0.0228	0.703972	0.703939	6.01	26.8	0.135475	0.512913	6.2	463	0.29	4.66	0.00875	0.283044	11.2	372	
Duomaohe	12LZ25	3.2	813	0.0114	0.704136	0.70412	7.99	38.8	0.124613	0.512853	5.1	508	0.21	5.7	0.00533	0.282978	9.2	439	
	12LZ26	3.18	877	0.0105	0.704341	0.704326	8.25	38.8	0.128461	0.512857	5.1	525	0.24	5.72	0.00607	0.282978	9.1	449	

12LZ28	3.68	826	0.0129	0.704319	0.7043	8.04	38.1	0.127667	0.512849	5	534	0.22	5.55	0.00572	0.282969	8.8	459	-0.22
12LZ23	3.71	844	0.0127	0.704123	0.704105	8.2	39.7	0.125003	0.512856	5.2	506	0.23	5.79	0.00569	0.282977	9.1	446	-0.33
12LZ29	4.08	828	0.0143	0.704133	0.704113	8.22	39.7	0.125253	0.512858	5.2	504	0.24	5.9	0.00589	0.282978	9.1	447	
12LZ30	3.79	867	0.0126	0.704264	0.704246	8.46	40.1	0.127666	0.512854	5.1	526	0.23	5.81	0.00575	0.282975	9	451	-0.35

Note Sr-Nd-Hf-Mg isotope data are from Dai et al., (2014, 2017; 2018)

Table. 4. The element concentrations and isotopic ratios of all endmembers used for the modeling are in Fig. 3A.

	Li (μg/g)	δ^7Li (‰)	Sr (μg/g)	$^{87}Sr/^{86}Sr$
Mantle	1.5	3.5	21.1	0.7026
Altered oceanic crust	8	13	110	0.7052
Carbonates	1.5	25	220	0.709
Silicate sediments	74	-4.5	120	0.708

Notes the values of Li and Sr contents and their isotopic composition for the mantle are from Marschall et al. (2017); Salters and Stracke, (2004), for the carbonates are from Penniston-Dorland et al. (2017); Wang et al. (2018); for the altered oceanic crust are from Chan et al. (1992, 2002); Zhou et al. (2014); Wang et al. (2018) for the silicate sediments are from Tang et al. (2014); Tian et al. (2020).

FIGURES DR1-6

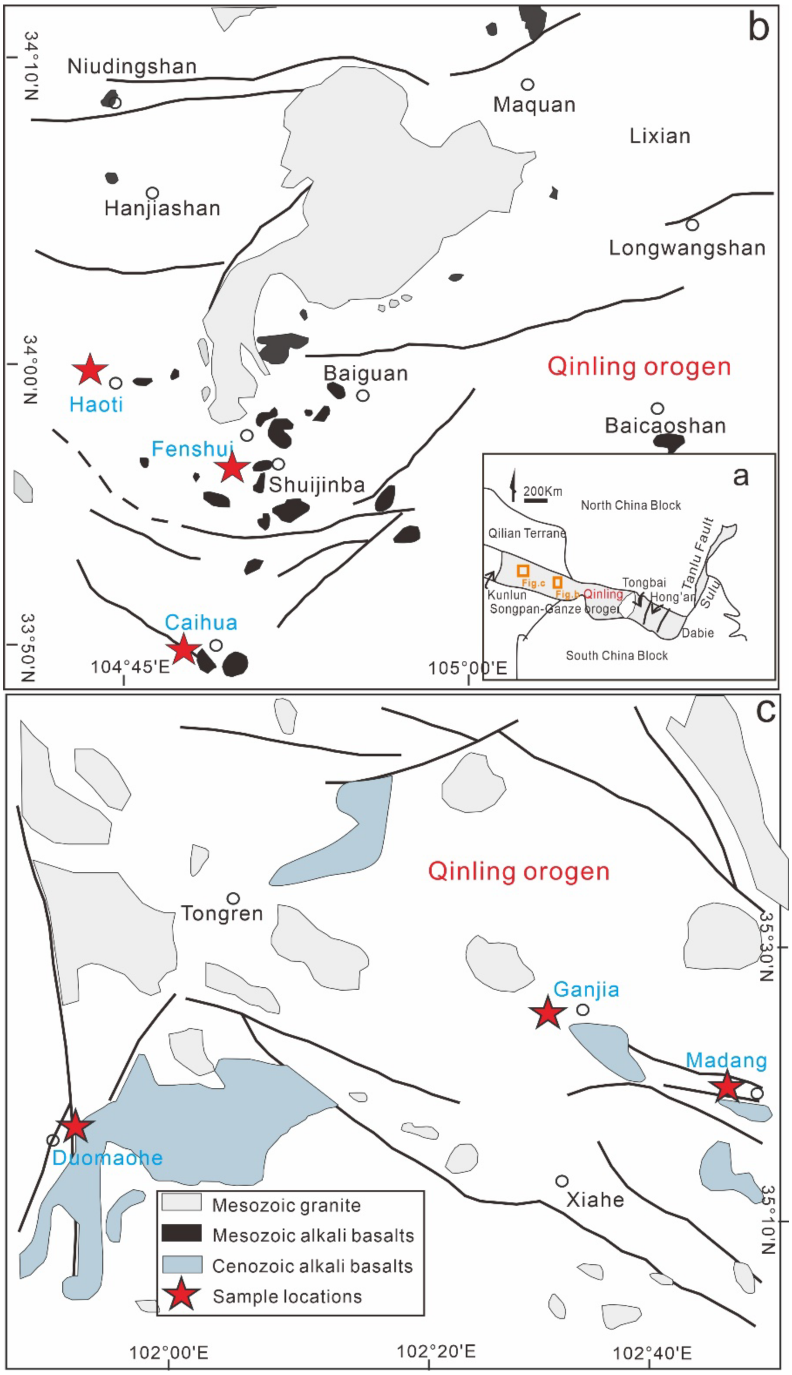

Figure 1. The geological information of the Cenozoic alkali basalts and Mesozoic alkali basalts and from the West Qingling orogen, modified after Dai et al., (2017). The Qingling orogen, located in central China, is a production of a series of tectonic processes from oceanic subduction and arc-continental subduction in the Paleozoic to continental-continental collision in the Early Mesozoic (Wu and Zheng, 2013; Dong and Santosh, 2016). This orogen is

commonly subdivided into the East Qinling orogen and the West Qinling orogen by the Baoji-Chengdu railway. The main rock types contain sedimentary cover, voluminous granitoid, and a certain amount of volcanic rocks, and the latter is dominated composed of alkali basalts, andesite, and rhyolite (Dai et al., 2014). In particular, these alkali basalts provide a good opportunity to probe into the nature of the mantle source under the Qinling orogen and uncover the metasomatic types occurring in the Paleotehyan oceanic subduction channel.

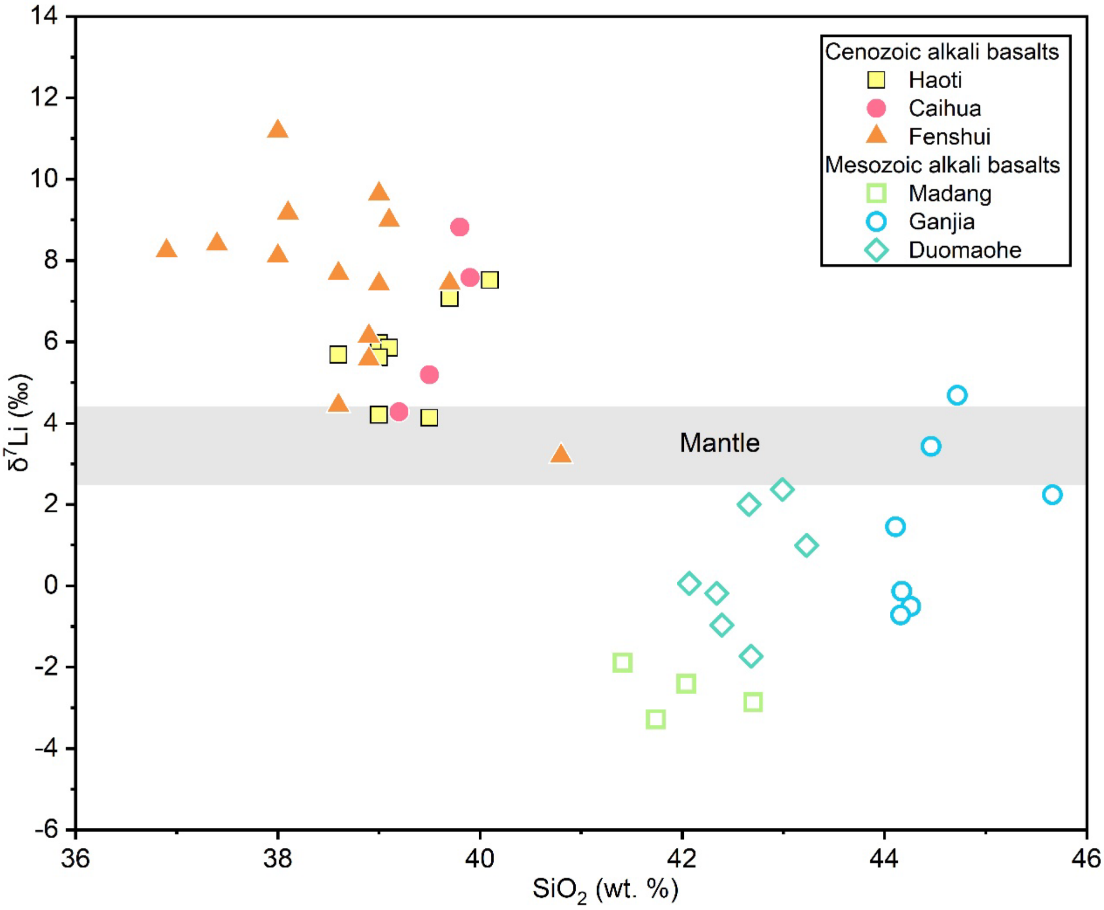

Figure 2. The plot of δ^7Li vs. SiO_2. There is no correlation between δ^7Li value and SiO_2 content indicating that the Li isotopic compositions of the investigated alkali basalts samples were not modified by crustal contamination.

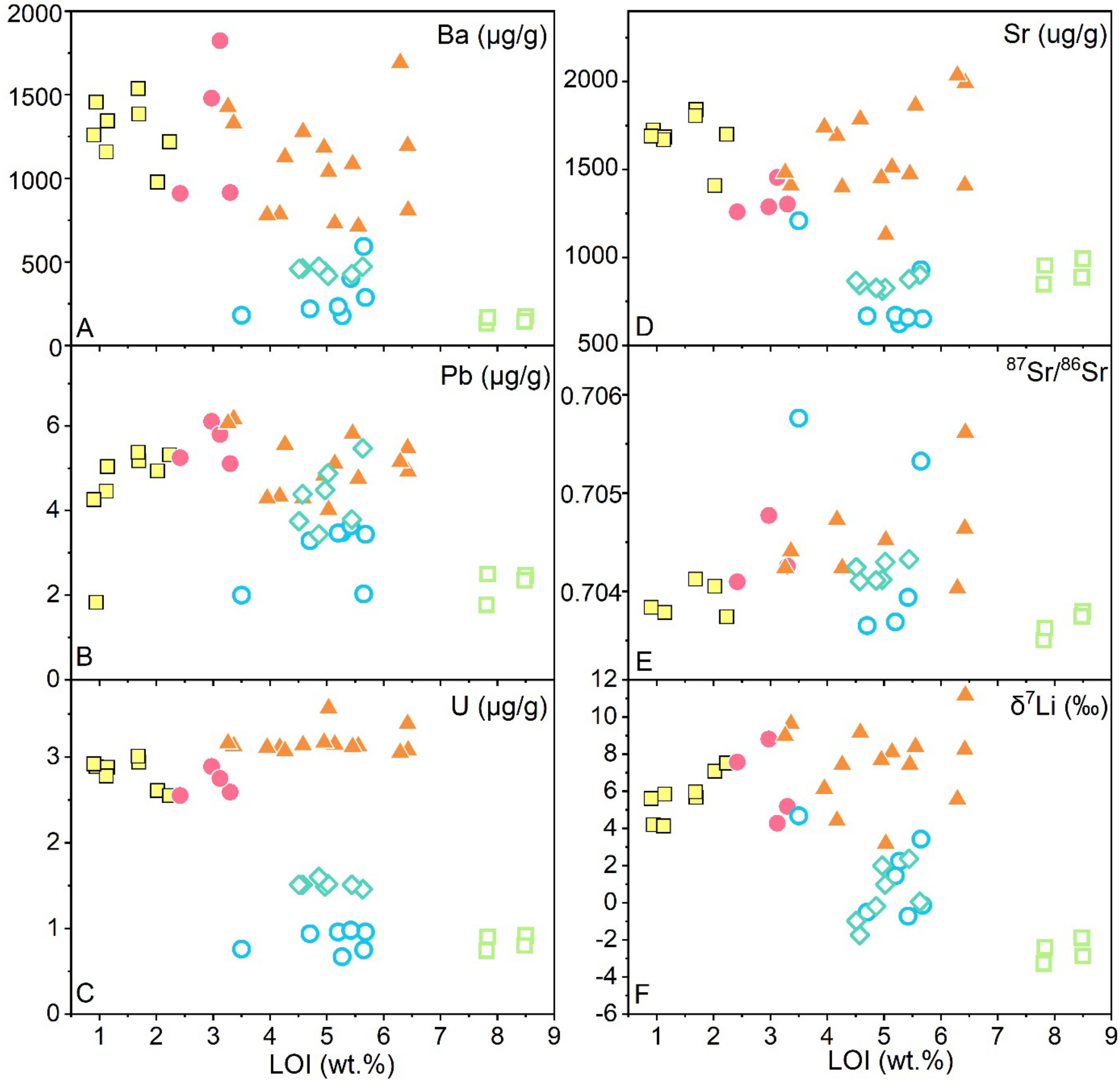

Figure 3. Plots of LOI values versus Ba, Pb, U, and Sr contents and Sr-Li isotopic ratios for two series of basalts from West Qinling orogen. There are no correlations between LOI values and Ba, Pb, U, and Sr contents as well as Sr-Li isotopic ratios, indicating the weathering process has a limited influence on the element and isotope compositions of the studied basalts.

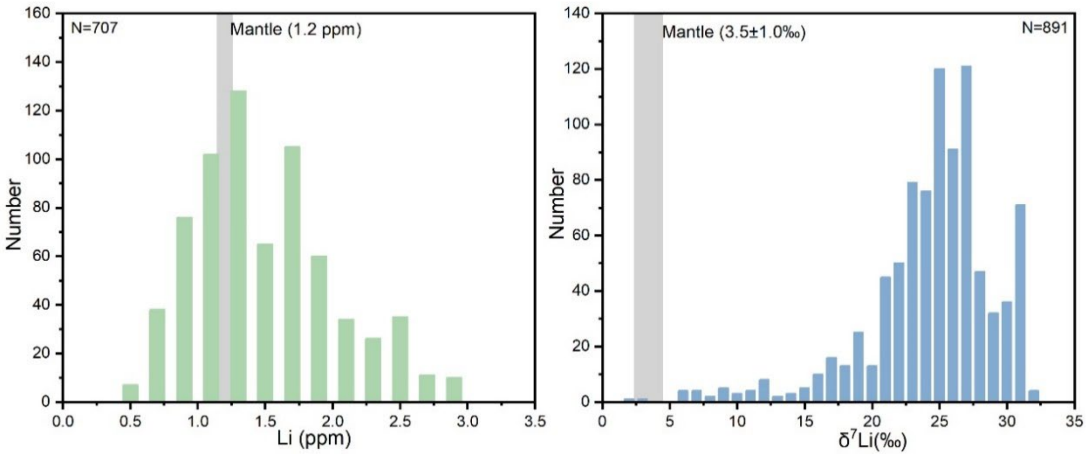

Figure 4. A comparison of Li contents and δ^{7}Li values for the marine carbonates (You and Chan, 1996; Marriott et al., 2004; Misra et al., 2012; Pogge et al., 2013, 2019; Lechler et al., 2015; Sun et al., 2018; Dellinger et al., 2020) and mantle (Marschall et al., 2017).

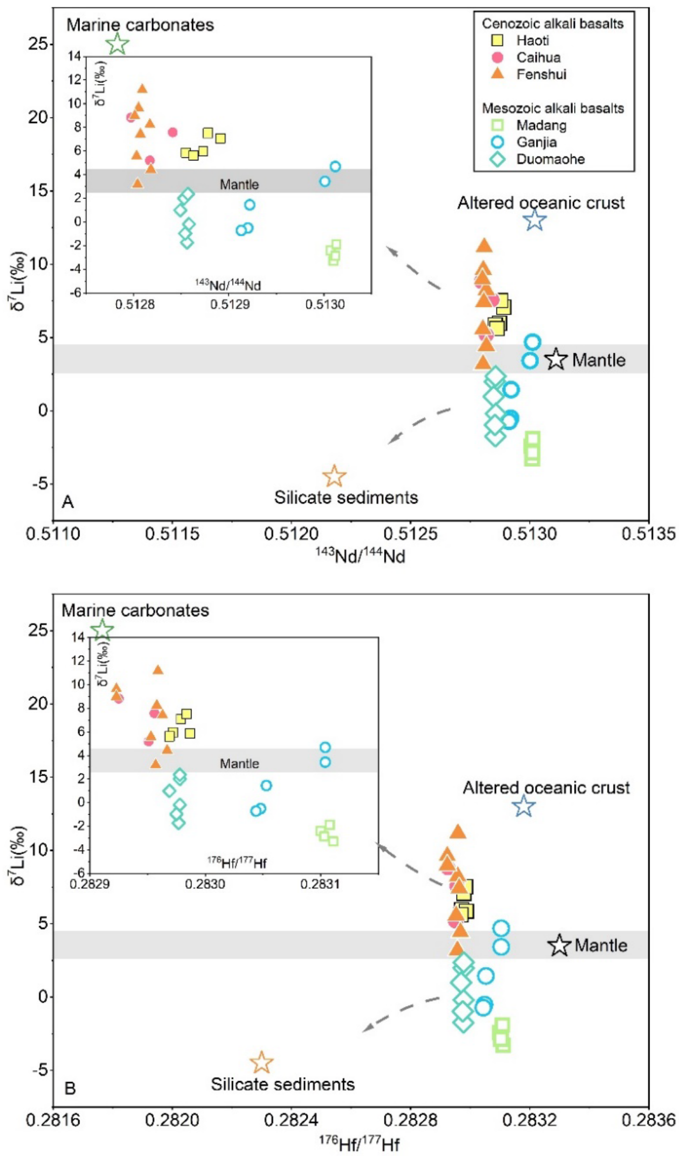

Figure 5. The plots of δ^7Li values vs. ^{143}Nd/^{144}Nd and ^{166}Hf/^{177}Hf values. The ^{143}Nd/^{144}Nd and ^{166}Hf/^{177}Hf values of Cenozoic and Mesozoic basalts fall closer to the carbonate and silicate sediments, respectively, than to the oceanic crust.

Notes: the δ^7Li, ^{143}Nd/^{144}Nd, and ^{166}Hf/^{177}Hf values for the mantle are from Marschall et al. (2017); Salters and Stracke, (2004), for the silicate sediments are from Plank et al., (2014); Tang et al. (2014), for the carbonates are from Penniston-Dorland et al. (2017); Wang et al. (2018); for the altered oceanic crust are from Chan et al. (1992, 2002); Zhou et al. (2014).

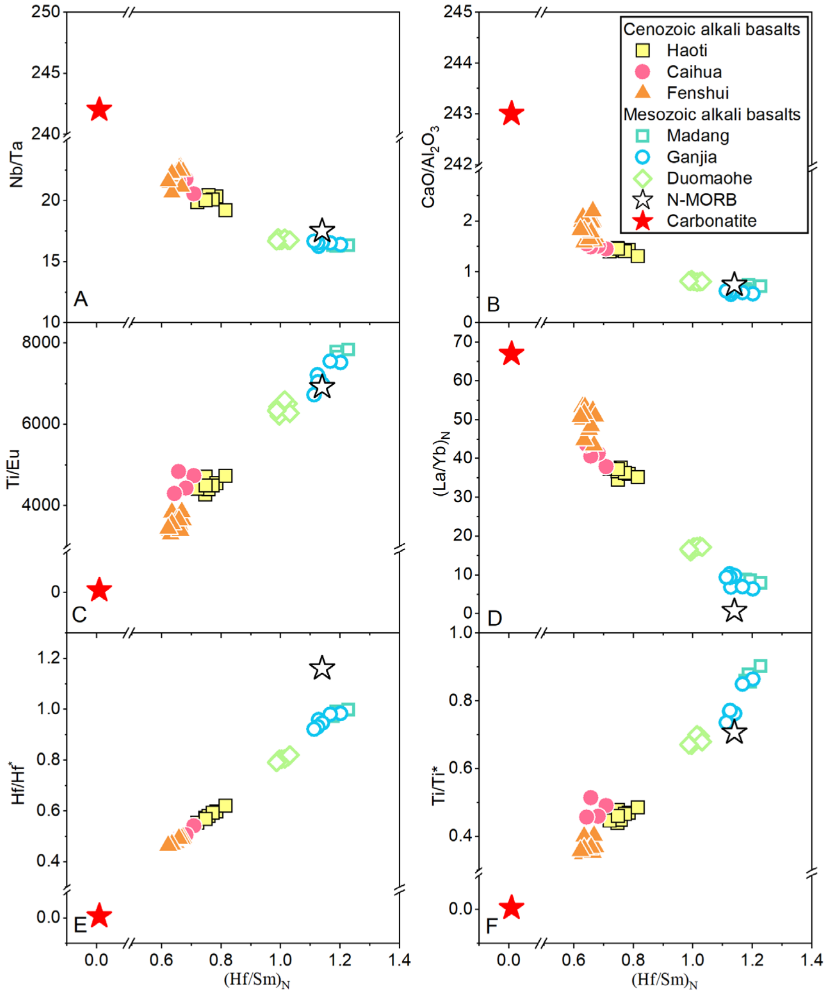

Figure 6. Variation of $(Hf/Sm)_N$ vs. Nb/Ta (A), CaO/Al_2O_3 (B), Ti/Eu (C), $(La/Yb)_N$ (D), Hf/Hf* (E), Ti/Ti* (F) for the Cenozoic alkali basalts and Mesozoic alkali basalts from West Qingling orogen, showing systemic differences in major-trace elemental features. Also shown

are the compositions of the MORB (Hofmann, 1988) and average oceanic carbonatite (Hoernle et al., 2002). The major and trace element compositions of the Cenozoic alkali basalts plot toward average carbonatite, whereas those of the Mesozoic alkali basalts are close to the MORB.

REFERENCES

Chan, L. H., Alt, J. C., and Teagle, D. A. H., 2002, Lithium and lithium isotope profiles through the upper oceanic crust: a study of seawater-basalt exchange at ODP Sites 504B and 896A: Earth and Planetary Science Letters, v. 201, no. 1, p. 187-201.

Chan, L. H., Edmond, J. M., Thompson, G., and Gillis, K., 1992, Lithium isotopic composition of submarine basalts: implications for the lithium cycle in the oceans Earth and Planetary Science Letters, v. 108, no. 1-3, p. 151-160.

Dai, L.-Q., Zhao, Z.-F., and Zheng, Y.-F., 2014, Geochemical insights into the role of metasomatic hornblendite in generating alkali basalts: Geochemistry, Geophysics, Geosystems, v. 15, no. 10, p. 3762-3779.

Dai, L.-Q., Zhao, Z.-F., Zheng, Y.-F., An, Y.-J., and Zheng, F., 2017, Geochemical Distinction between Carbonate and Silicate Metasomatism in Generating the Mantle Sources of Alkali Basalts: Journal of Petrology, v. 58, no. 5, p. 863-884.

Dai, L.-Q., Zheng, F., Zhao, Z.-F., and Zheng, Y.-F., 2018, Geochemical insights into the lithology of mantle sources for Cenozoic alkali basalts in West Qinling, China: Lithos, v. 302-303, p. 86-98.

Dellinger, M., Hardisty, D. S., Planavsky, N. J., Gill, B. C., Kalderon-Asael, B., Asael, D., Croissant, T., Swart, P. K., and West, A. J., 2020, The effects of diagenesis on lithium isotope ratios of shallow marine carbonates: American Journal of Science, v. 320, no. 2, p.

150-184.

Dong, Y., and Santosh, M., 2016, Tectonic architecture and multiple orogeny of the Qinling Orogenic Belt, Central China: Gondwana Research, v. 29, no. 1, p. 1-40.

Hoernle, K., Tilton, G., Le Bas, M. J., Duggen, S., and Garbe-Schönberg, D., 2002, Geochemistry of oceanic carbonatites compared with continental carbonatites: mantle recycling of oceanic crustal carbonate: Contributions to Mineralogy and Petrology, v. 142, no. 5, p. 520-542.

Hofmann, A. W., 1988, Chemical differentation of the Earth - The relationship between mantle, continental-crust and oceanic-crust: Earth and Planetary Science Letters, v. 90, no. 3, p. 297-314.

Lechler, M., Pogge von Strandmann, P. A. E., Jenkyns, H. C., Prosser, G., and Parente, M., 2015, Lithium-isotope evidence for enhanced silicate weathering during OAE 1a (Early Aptian Selli event): Earth and Planetary Science Letters, v. 432, p. 210-222.

Magna, T., Wiechert, U., and Halliday, A. N., 2006, New constraints on the lithium isotope compositions of the Moon and terrestrial planets: Earth and Planetary Science Letters, v. 243, no. 3-4, p. 336-353.

Marriott, C. S., Henderson, G. M., Belshaw, N. S., and Tudhope, A. W., 2004, Temperature dependence of delta Li-7, delta Ca-44 and Li/Ca during growth of calcium carbonate: Earth and Planetary Science Letters, v. 222, no. 2, p. 615-624.

Marschall, H. R., Wanless, V. D., Shimizu, N., Pogge von Strandmann, P. A. E., Elliott, T., and Monteleone, B. D., 2017, The boron and lithium isotopic composition of mid-ocean ridge basalts and the mantle: Geochimica et Cosmochimica Acta, v. 207, p. 102-138.

Misra, S., and Froelich, P. N., 2012, Lithium Isotope History of Cenozoic Seawater: Changes in Silicate Weathering and Reverse Weathering: Science, v. 335, no. 6070, p. 818-823.

Penniston-Dorland, S., Liu, X.-M., and Rudnick, R. L., 2017, Lithium Isotope Geochemistry: Reviews in Mineralogy and Geochemistry, v. 82, no. 1, p. 165-217.

Pogge von Strandmann, P. A. E., Jenkyns, H. C., and Woodfine, R. G., 2013, Lithium isotope evidence for enhanced weathering during Oceanic Anoxic Event 2: Nature Geoscience, v. 6, no. 8, p. 668-672.

Pogge von Strandmann, P. A. E., Schmidt, D. N., Planavsky, N. J., Wei, G., Todd, C. L., and Baumann, K.-H., 2019, Assessing bulk carbonates as archives for seawater Li isotope ratios: Chemical Geology, v. 530, p. 119338.

Salters, V. J. M., and Stracke, A., 2004, Composition of the depleted mantle: Geochemistry, Geophysics, Geosystems, v. 5, no. 5.

Sun, H., Xiao, Y. L., Gao, Y. J., Zhang, G. J., Casey, J. F., and Shen, Y. A., 2018, Rapid enhancement of chemical weathering recorded by extremely light seawater lithium isotopes at the Permian-Triassic boundary: Proceedings of the National Academy of Sciences of the United States of America, v. 115, no. 15, p. 3782-3787.

Tang, M., Rudnick, R. L., and Chauvel, C., 2014, Sedimentary input to the source of Lesser Antilles lavas: A Li perspective: Geochimica Et Cosmochimica Acta, v. 144, p. 43-58.

Tian, H. C., Teng, F. Z., Hou, Z. Q., Tian, S. H., Yang, W., Chen, X. Y., and Song, Y. C., 2020, Magnesium and Lithium Isotopic Evidence for a Remnant Oceanic Slab Beneath Central Tibet: Journal of Geophysical Research-Solid Earth, v. 125, no. 1.

Wang, X. J., Chen, L. H., Hofmann, A. W., Hanyu, T., Kawabata, H., Zhong, Y., Xie, L. W., Shi,

J. H., Miyazaki, T., Hirahara, Y., Takahashi, T., Senda, R., Chang, Q., Vaglarov, B. S., and Kimura, J. I., 2018, Recycled ancient ghost carbonate in the Pitcairn mantle plume: Proc Natl Acad Sci U S A, v. 115, no. 35, p. 8682-8687.

Wu, Y.-B., and Zheng, Y.-F., 2013, Tectonic evolution of a composite collision orogen: An overview on the Qinling–Tongbai–Hong'an–Dabie–Sulu orogenic belt in central China: Gondwana Research, v. 23, no. 4, p. 1402-1428.

You, C. F., and Chan, L. H., 1996, Precise determination of lithium isotopic composition in low concentration natural samples: Geochimica Et Cosmochimica Acta, v. 60, no. 5, p. 909-915.

Zhou, L.-G., Xia, Q.-X., Zheng, Y.-F., and Hu, Z., 2014, Polyphase growth of garnet in eclogite from the Hong'an orogen: Constraints from garnet zoning and phase equilibrium: Lithos, v. 206, p. 79-99.